Neurochemical Research (2025) 50:135
https://doi.org/10.1007/s11064-025-04379-x

RESEARCH

Targeting UAF1 Alleviate Neurotoxicity by Inhibiting APP/NLRP3 Axis-Mediated Pyroptosis and Apoptosis

Ling Cheng[1] · Xianguang Meng[2] · Dandan Tian[1] · Bin Zheng[1] · Yinfan Xiao[1] · Xueying Zhao[3] · Yingying Xu[1] · Hui Yang[1] · Jianzhong Bi[1] · Fan Li[1] · Zhaohong Xie[1]

Received: 18 September 2024 / Revised: 17 March 2025 / Accepted: 18 March 2025 / Published online: 4 April 2025

Abstract
The accumulation of amyloid β (Aβ) protein, derived from the amyloid precursor protein (APP), plays a pivotal role in the pathogenesis of Alzheimer's disease (AD) by inducing neuronal cell injury. This study investigated the specific functions of ubiquitin-specific protease 1-associated factor 1 (UAF1) in mediating the neurotoxic effects triggered on Aβ. To model AD-related neuronal injury in vitro and in vitro, SH-SY5Y cells exposed to $A\beta_{25-35}$ and APPswe/PS1dE9 (APP/PS1) transgenic mice were utilized. Compared with control mice, UAF1 levels were significantly elevated in the hippocampus of experimental mice. In vitro experiments showed that UAF1 knockdown reduced Aβ-induced apoptosis and enhanced cell viability. Furthermore, UAF1 knockdown markedly suppressed $A\beta_{25-35}$ -induced pyroptosis in SH-SY5Y cells and reduced the production of IL-1β and IL-18 through the nucleotide-binding domain and leucine-rich repeat containing family pyrin domain-containing 3 (NLRP3)/Gasdermin D pathway. Mechanistic analyses revealed that UAF1 directly binds to NLRP3 to mediate its effects. In vivo, UAF1 knockdown mitigated cognitive deficits, decreased APP expression, Aβ plaque deposition, and reduced hyperphosphorylated Tau levels. These findings underscore the critical role of UAF1 in regulating neuronal apoptosis and pyroptosis, thereby highlighting its potential as a promising therapeutic target for AD.

Keywords Alzheimer's disease (AD) · Aβ · UAF1 · NLRP3 · Pyroptosis · Apoptosis

Introduction

Alzheimer's disease (AD) is a multifactorial degenerative neurological disorder recognized as a significant global health concern. Characterized by progressive impairment of cognition, memory, and behavioral dynamics in the elderly, AD poses substantial challenges to individuals, families, and healthcare systems worldwide. Despite advancements in understanding the mechanisms underlying AD, much remains to be clarified. Continued research and innovative therapeutic strategies are crucial for improving AD treatment outcomes.

The hallmark pathological features of AD include amyloid β (Aβ) plaque aggregation and the propagation of tau pathology. These abnormal protein aggregates disrupt neuronal communication and lead to neuronal death, resulting in the cognitive decline characteristic of AD. Evidence suggests that Aβ treatment induces neuronal apoptosis and pyroptosis, with growing support indicating that nucleotide-binding domain and leucine-rich repeat containing family pyrin domain -containing 3 (NLRP3) inflammasome-mediated pyroptosis is closely linked to AD pathogenesis, particularly through neuroinflammation [1–4]. The NLRP3 inflammasome acts as a critical trigger for pyroptosis by promoting caspase-1 activation, which facilitates the release of pro-inflammatory factors such as interleukin-1 beta (IL-1β)

Zhaohong Xie and Fan Li contributed equally to this work.

✉ Fan Li
201162013888@email.sdu.edu.cn

✉ Zhaohong Xie
xie_zhaohong@sdu.edu.cn

[1] Department of Neurology Medicine, The Second Hospital of Shandong University, Jinan, Shandong Province 250033, China

[2] Department of Dermatology, Central Hospital Affiliated to Shandong First Medical University, 105 Jiefang Street, Jinan 250013, China

[3] Department of Blood Transfusion, The Second Hospital of Shandong University, Jinan, Shandong Province 250033, China

and interleukin-18 (IL-18). This process leads to gasdermin D (GSDMD)-mediated pore formation and cell lysis, resulting in inflammation and pyroptosis, ultimately contributing to neuronal dysfunction and death [5]. While NLRP3 is primarily associated with microglial pyroptosis [6], research on its role in neuronal pyroptosis remains limited. Preliminary studies have demonstrated that Aβ treatment induces NLRP3 inflammasome-triggered neuronal pyroptosis in neuronal cell lines and cultured mouse cortical neurons [7, 8], with similar findings observed in aging-accelerated mice [9]. Therefore, targeting NLRP3 inflammasome-regulated neuronal pyroptosis holds promise as a therapeutic strategy for mitigating AD.

Ubiquitin-associated factor 1 (UAF1), also known as WD repeat domain 48 (WDR48), is a multifunctional protein that collaborates with ubiquitin-specific proteases to regulate protein degradation, maintain cellular homeostasis, and influence various signaling pathways related to immune responses [10, 11]. Previous studies have shown that the USP1-UAF1 complex binds to TBK1, enhancing IFN-β secretion by removing K48-linked polyubiquitination [10]. UAF1 modulates the activity of nuclear factor-kappa B (NF-κB)-dependent gene expression and pro-inflammatory cytokine production by regulating P65 ubiquitination. Additionally, UAF1 has been implicated in modulating NLRP3 inflammasome complexes by altering the ubiquitination status of NLRP3 [11]. Emerging evidence suggests that UAF1 knockdown alleviates SEV-induced cognitive impairment and neurotoxicity by suppressing neuroinflammation [12]. However, the precise molecular interactions underlying these effects remain unclear.

In this study, our findings revealed that UAF1 levels were elevated in $A\beta_{25-35}$-treated SH-SY5Y cells. Knocking down UAF1 enhanced SH-SY5Y cell proliferation and reduced Aβ-induced pyroptosis. Mechanistic analysis indicated that UAF1 directly interacts with NLRP3. Furthermore, UAF1 knockdown significantly improved AD-related pathological features and ameliorated cognitive deficits in APP/PS1 mice.

Materials and Methods

Reagents and Antibodies

$A\beta_{25-35}$ and $A\beta_{42}$ were obtained from Med Chem Express (Monmouth Junction, NJ, USA). SH-SY5Y cells were treated with $A\beta_{25-35}$ and $A\beta_{1-42}$ at concentrations of 40 μM and 20 μM, respectively. The SH-SY5Y cells were acquired from the Cell Center of the Chinese Academy of Medical Sciences (Beijing, China) and cultured in Dulbecco's Modified Eagle Medium (DMEM, Gibco, California, USA) supplemented with 10% fetal bovine serum (FBS) and 1% penicillin-streptomycin (Solarbio, Beijing, China) under standard conditions of 5% CO_2 at 37 °C. NLRP3 (cat. no.15101s), p-P65 (cat.no.3033s), and P65 (cat.no.8242s) were purchased from Cell Signaling Technology (Danvers, MA, USA). UAF1 (cat.no. A6854) was obtained from ABclonal (Wuhan, China). Iba1 (cat.no.sc32725) and GFAP (cat.no.sc33673) were purchased from Santa Cruz Biotechnology (Beverly, MA, USA). Hyperphosphorylated Tau (p-Tau) (cat.no.28866-1-AP), NeuN (cat.no.66836-1-Ig), β-actin (cat.no.20536-1-AP), GSDMD (cat.no.20770-1-AP), MYC tag (cat.no. 16286-1-AP), Flag tag (cat. no.66008-4-Ig), and IgG (cat.no.30000-0-AP) were obtained from Proteintech Group, Inc. (Wuhan, China). Aβ (cat. no. ab201060) and APP (cat.no. ab32136) were purchased from Abcam (Cambridge, USA). iFluor^{TM}488-conjugated goat anti-rabbit IgG polyclonal antibody (cat.no. HA1121), HRP peroxidase-conjugated goat anti-mouse antibody (cat. no. HA1006), and HRP peroxidase-conjugated goat anti-rabbit antibody (cat.no. HA1001) were obtained from HuaBio (Hangzhou, China). DyLight 549 goat anti-mouse IgG (cat.no. A23310) and DyLight 594 goat anti-rabbit IgG (cat. no. A23420) were purchased from Abbkine Scientific Co. (Wuhan, China). The lentivirus-sh-UAF1 and adeno-associated virus (AAV)-sh-UAF1 were obtained from GENEchem (Shanghai, China).

Solid $Abeta_{25-35}$ and $Abeta_{42}$ were dissolved in cold hexafluoro-2-propanol (HFIP). The peptide was incubated at room temperature for at least 1 h to ensure monomerization and structural randomization. The HFIP was then removed by evaporation, and the resulting film was dissolved in anhydrous DMSO at 5 mM and subsequently diluted to the appropriate concentration and buffer (serum- and phenol-red-free culture medium) with vortexing. The solution was aged for 48 h at 4–8 °C. After aging, the sample was centrifuged at 14,000 g for 10 min at 4–8 °C, and the soluble oligomers were collected in the supernatant. The supernatant was further diluted for experiments.

Mice

Wild-type (WT, 5-month-old, male) C57BL/6J mice were obtained from Beijing Vital River Laboratory Animal Technology Co., Ltd. (Beijing, China). APP/PS1 mice (5-month-old, male) were acquired from HFK Biosciences (Beijing, China). All mice were maintained under a standard 12-hour light/dark cycle with unrestricted access to food and water. All experiments complied with the Guidelines on the Care and Use of Laboratory Animals, and all animal protocols were approved by the ethics committee of The Second Hospital of Shandong University (KYLL-2021(KJ)A-0195).

Cell Transfection

SH-SY5Y cells were seeded in a 24-well plate (1×10^5 cells per well) and infected with a lentivirus to knockdown UAF1 (LV-sh-UAF1). The infected cells were selected with 2 μg/ml puromycin for 3 days to obtain a stable cell line for subsequent experiments [13].

Stereotactic Injection

APP/PS1 mice underwent hippocampal injection with either AAV-sh-UAF1 or AAV-sh-NC using a stereotaxic injection technique. Two small holes were drilled for AAV injection. The coordinates used for the AAV injection into the hippocampus were AP: 2.0 mm, ML: ±1.7 mm, DV: −1.9 mm. The mice were anesthetized with 3% isoflurane and positioned on a stereotactic apparatus. A total of 2 μL of AAV-virus (~10^{12} infection units per mL) was injected at a rate of 0.2 μL/min. The needle was maintained in place for 10 min post-injection. After the procedure, the animals were returned to their hutches until behavioral studies were performed.

Quantitative Real-Time Polymerase Chain Reaction (qRT-PCR)

Total RNA was isolated using the RNeasy Isolation Kit (Tiangen, Beijing, China) and reverse-transcribed into cDNA with the First Strand cDNA Synthesis Kit (Tiangen). The qRT-PCR amplification procedure was conducted using SYBR qPCR Master Mix (Tiangen). The relative expression levels of inflammatory factors were analyzed using the $2^{-\Delta\Delta CT}$ method and normalized to glyceraldehyde 3-phosphate dehydrogenase (GAPDH). The primer sequences used in these experiments are listed in Table 1:

Reactive Oxygen Species (ROS)

The levels of ROS in SH-SY5Y cells were determined using the ROS assay kit (Beyotime, Shanghai, China) in accordance with the supplier's instructions. Briefly, dichlorodihydrofluorescein diacetate (DCFH-DA) was diluted in the medium at a ratio of 1:1000. Then, 10 μL of the diluted DCFH-DA was added to each well containing treated cells, followed by incubation for 20 min at 37 °C. After incubation, the DCFH-DA residue was removed, and the cells were washed. A fluorescence microscope was then used to detect 2',7'-dichlorofluorescein (DCF), and images were captured.

Table 1 The primer sequences

Gene	Forward Primer (5'-3')	Reverse Primer (5'-3')
UAF1	GCCAGGACCAGGTTTTG GAT	ACGGTAATGGAGG GTGAGGT
IL-18	ATTGACCAAGGAAATCG GCCTC	GGTCCGGGGTGCA TTATCTCT
IL-1β	CAACAAGTGGTGTTCTCC ATGTC	ACACGCAG-GACA GGTACAGA
NLRP3	GATCTTCGCTGCGATCA ACA	GGGATTCGAAACA CGTGCATTA
GAPDH	AACGGATTTGGTCG-TAT TGGG	CCTGGAAGATGG-T AATGGGAT

Enzyme-Linked Immunosorbent Assay (ELISA)

The production of IL-1β and IL-18 in SH-SY5Y cells was examined using ELISA kits [14] (MultiSciences Biotech, Co., Ltd., Hangzhou, China;) following the supplier's instructions.

Immunofluorescence

For SH-SY5Y cell immunofluorescence (IF), the processed cells were incubated with anti-p-P65 for 12 h at 4 °C after fixation, blocking, and permeabilization. Thereafter, the cells were incubated with the corresponding secondary antibody at room temperature and stained with 4′, 6-diamidino-2-phenylindole (DAPI) for nuclear visualization.

For tissue IF, the sections were fixed with 4% paraformaldehyde (PFA) and blocked at room temperature with 5% goat serum containing 0.1% TritonX-100. The sections were then incubated with primary antibodies for 12 h at 4 °C, followed by incubation with iFluor™ 488 or DyLight 549-conjugated secondary antibodies, and counterstained with DAPI for nuclear visualization. Images were captured using a multispectral imaging system (Mantra).

Western Blot

Processed cells or tissues were collected and lysed using a radioimmunoprecipitation assay buffer (Solarbio, Beijing, China) containing 0.1% protease inhibitor (Solarbio), and protein concentrations were measured using the BCA Protein Quantification Kit (Vazyme, Nanjing, China). Equal amounts of samples (10 μg) were then separated and transferred as previously described. After incubation with the appropriate antibodies, an enhanced chemiluminescent (ECL) reagent was applied to develop the protein bands, and the relative densitometry values were estimated using ImageJ software.

Cell Viability Assay

The Cell Counting Kit-8 (CCK-8) assay was used to evaluate the growth ability of SH-SY5Y cells. A total of 3000 treated cells were seeded in 96-well plates, and the optical

density (OD) value was measured every 24 h after adding CCK-8 solution to each well. The growth curve was generated using GraphPad Prism 9.

Colony Formation Assay

For the colony formation assay, cells were harvested and seeded onto a six-well plate at a density of 1000 cells per well and cultured for 2 weeks. After fixation with paraformaldehyde (5 min) and staining with crystal violet (20 min), the colonies were imaged and counted.

Flow Cytometry

After treating SH-SY5Y cells with Aβ, the cells were harvested and washed twice with PBS. The cells were then resuspended in Annexin V-PE/7-AAD and incubated away from light at 37 °C for 10 min, following the manufacturer's instructions provided with the Apoptosis Detection Kit (Vazyme).

Co-Immunoprecipitation (co-IP) Assay

For the co-immunoprecipitation (co-IP) assay, SH-SY5Y cells were seeded in 10 cm dishes and transiently co-transfected the following day with 5 µg of Myc-NLRP3 and 5 µg of Flag-UAF1 or 5 µg of an empty vector using Lipo2000 transfection reagent. After collection, the cellular extracts were incubated for 12 h at 4 °C with anti-Myc tag primary antibody and Protein A/G agarose beads (cat.no.sc2003). The precipitates were collected, eluted with 50 µL of SDS loading buffer, and processed for western blot analysis.

For endogenous proteins, Aβ-treated SH-SY5Y cells were collected and lysed. Cell lysates were incubated with anti-NLRP3 IgG antibody and Protein A/G agarose overnight at 4 °C. The precipitates were collected and eluted with 50 µL of SDS loading buffer, followed by western blot analysis.

Morris Water Maze (MWM) Test

The MWM test was used to evaluate cognitive function, including training (5 days) and probe trials (1 day). A circular tank (120 cm in diameter) was filled with water (60 cm deep), and a hidden platform was fixed and submerged 2 cm below the water surface. On spatial acquisition days 1–5, each mouse underwent four training sessions at 20-minute intervals and was allowed to locate the platform. The path taken by the mice and the time spent were recorded.

Statistical Analysis

All data obtained from triplicate experiments were presented as the mean ± standard deviation (SD) and analyzed using GraphPad Prism 9 software (GraphPad Software, Inc.). The Student's t-test was applied for comparisons between the two groups. Differences among three or more groups were analyzed using analysis of variance followed by Tukey's post hoc test. A single-blind trial was conducted for the MWM test. A P value less than 0.05 was considered statistically significant.

Results

UAF1 Was Up-Regulated in the Progression of AD

To examine the involvement of UAF1 in the pathology of AD, we first utilized the Human Protein Atlas database (https://www.proteinatlas.org) to analyze the expression of UAF1 in different cell types of brain tissue. UAF1 was uniformly expressed across various brain cell types without showing obvious cell specificity, consistent with immunofluorescence analysis in WT mice (Fig. 1A-1 and Fig. S1). The localization of UAF1 in the brain tissues of APP/PS1 mice was further analyzed by immunofluorescence. Interestingly, the analysis revealed that the UAF1 protein was primarily localized in neurons and microglia, with limited expression in GFAP-positive astrocytes in the brain tissues of APP/PS1 mice (Fig. 1A-1 and 1A-2). Compared to WT mice, the expression level of UAF1 in neurons was higher in APP/PS1 mice. Furthermore, compared to age-matched WT mice, UAF1 showed a gradual upregulation tendency with increasing age in APP/PS1 mice, an AD mouse model (Fig. 1B). Analysis from Fig. 1C exhibited that the accumulation of NLRP3, Tau, and p-Tau, which are important pathological features of AD, was increased in the brain tissue of experimental mice in comparison to control mice. UAF1 expression was positively correlated with NLRP3 and p-Tau levels (Fig. 1D). Additionally, we observed that UAF1 expression increased following $A\beta_{25-35}$ stimulation in SH-SY5Y cells (Fig. 1E), consistent with data obtained from $A\beta_{42}$ stimulation in SH-SY5Y cells (Fig. S2). Overall, these findings suggest that dynamic changes in UAF1 are potentially involved in the progression of AD.

Knockdown of UAF1 Improved Cognitive Impairment in Alzheimer's Mice

To further investigate the effect of UAF1 in AD development, we knocked-down UAF1 using AAV-sh-UAF1 in vivo. Four weeks after brain stereotactic injection, the

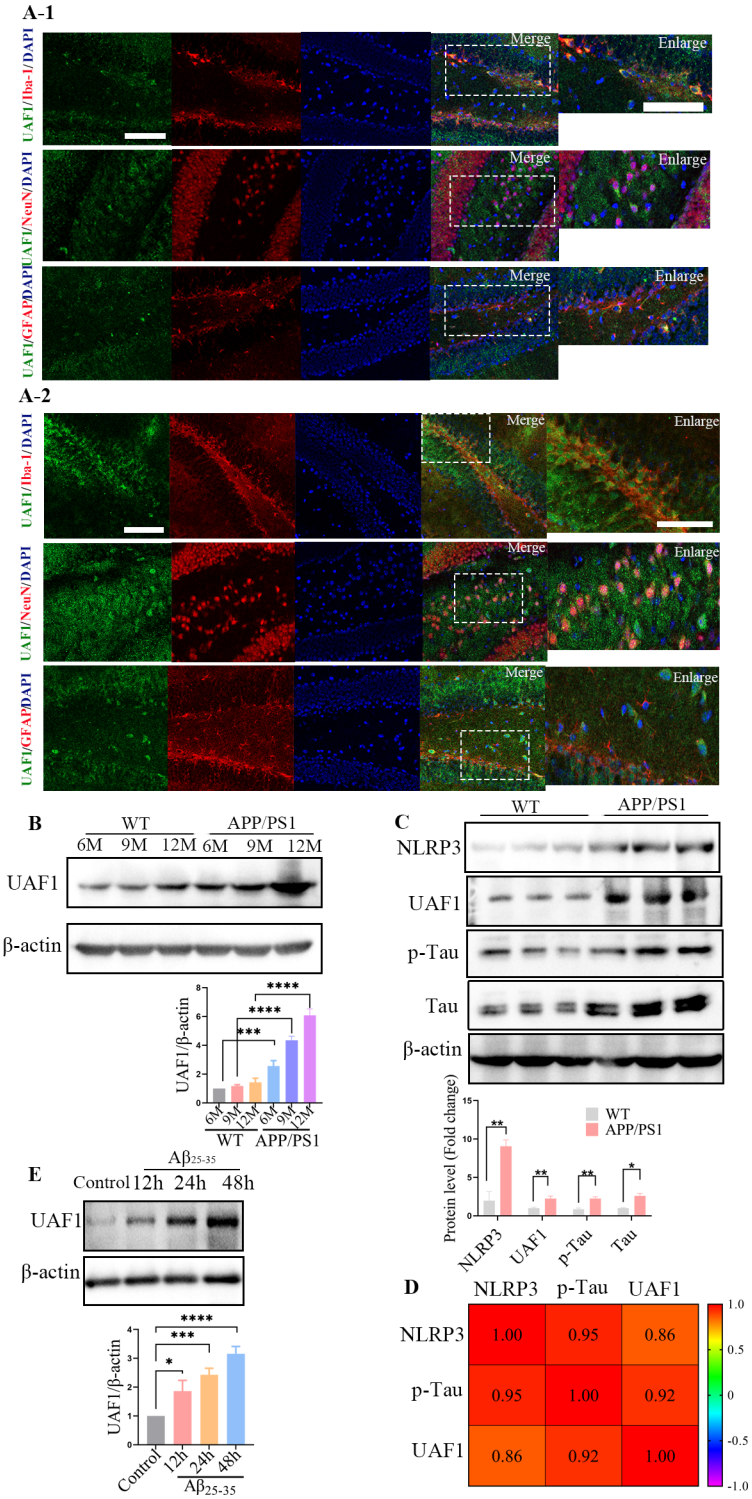

Fig. 1 Increased expression of UAF1 in APP/PS1 mice brains. (**A**) Immunofluorescent images of UAF1 (green), Iba1(red), GFAP (red), NeuN (red), and DAPI (blue) in the hippocampus from WT mice (A-1) and APP/PS1 mice (A-2) for 6 months old. Scale bar, 100 μm. (**B**) Immunoblots and quantification of UAF1 expression in the brain of WT and APP/PS1 mice for different months (6,9,12months old). (**C**) Immunoblots and quantification of NLRP3, UAF1, p-Tau and Tau expression in the hippocampus of WT and APP/PS1 mice for 6 months old ($n=6$ mice per group). (**D**) Pearson correlation analysis of UAF1, NLRP3, and p-Tau. (**E**) Immunoblots and quantification of UAF1 expression in $A\beta_{25\text{-}35}$-treated SH-SY5Y cells for the different time(The relevant experiments presented in this part were performed independently at least three times). Data are presented as mean±S.D. Statistical significance: * $p<0.05$, ** $p<0.01$, *** $p<0.001$, **** $p<0.0001$ vs. WT or Control group

knockdown efficiency was confirmed by western blotting (Fig. 2A and B). Subsequently, the MWM experiment was conducted to evaluate the cognitive performance of mice (Fig. 2C). During the initial 5-day MWM training period, the learning curves showed that at 6 months of age, the escape latency of experimental mice was higher than that of control mice. AAV-sh-UAF1 treatment reduced escape latency compared with the sh-NC group (Fig. 2D). Moreover, on the 6th day of the MWM test, UAF1 knockdown improved cognitive parameters, including reduced escape latency (Fig. 2E), a significant increase in entries to the target platform (Fig. 2F), and prolonged time spent in the

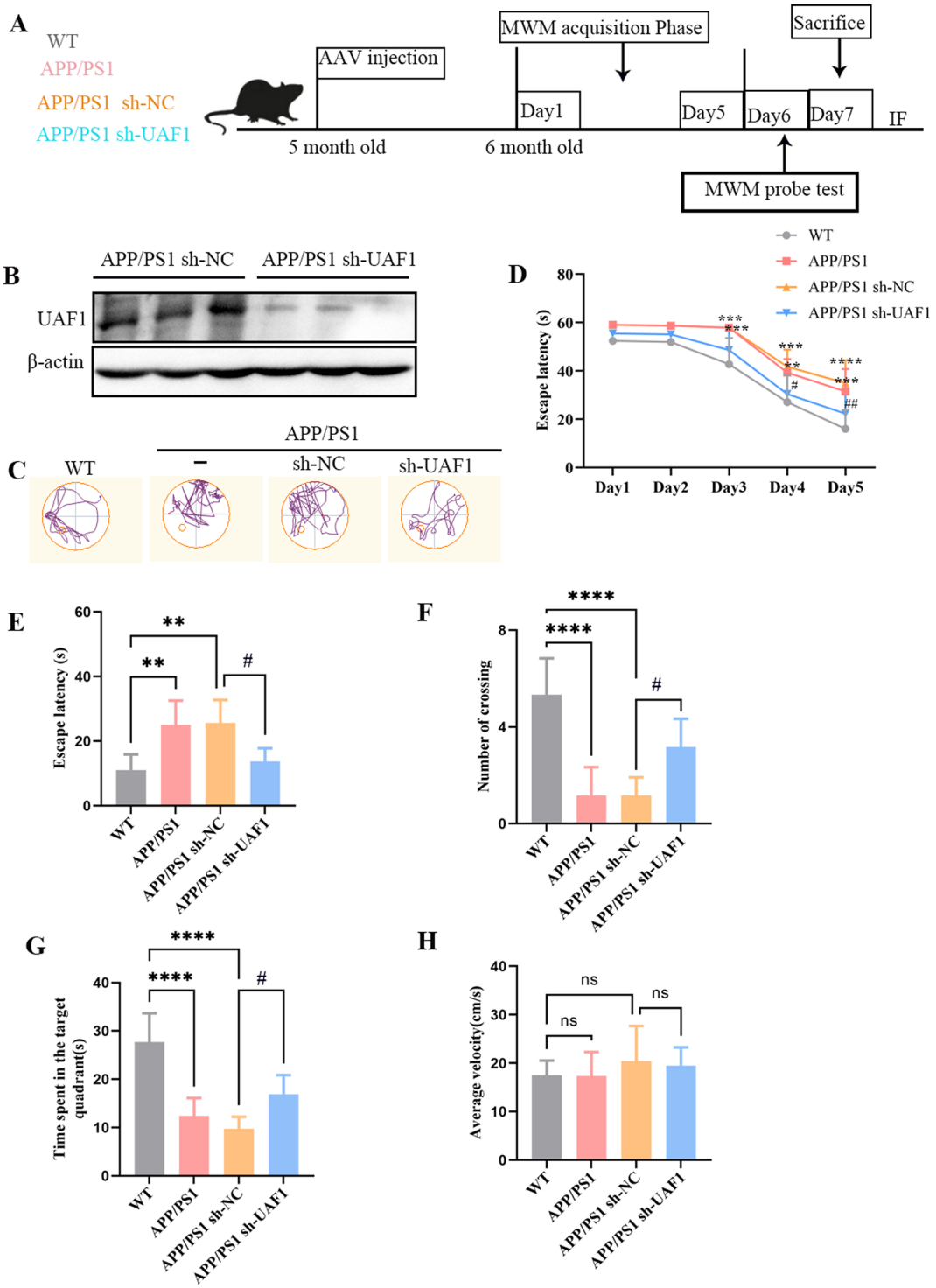

Fig. 2 Knockdown of UAF1 improved cognitive deficits in APP/PS1 mice. AAV-sh-NC or AAV-sh-UAF1 was injected into the 5-month APP/PS1 mice by the brain stereotactic apparatus, four weeks later, MWM test was performed, WT mice and APP/PS1 mice were the control group. (**A**) Experimental procedure of mice treatments. (**B**) Immunoblots of UAF1 knockdown efficiency in APP/PS1 mice. (**C**) Motion tracking of the MWM tests in the four groups. (**D**) Escape latency to reach the platform in the 1-5th training period. (**E**) Escape latency to reach the platform in the 6th test period. (**F**) The number of times crossing the target platform in the 6th test period. (**G**) Time spent in the target quadrant in the 6th test period. (**H**) Average swimming velocity in the four group. ($n=6$ mice per group). Statistical significance: $^{*}P<0.05$, $^{**}P<0.01$, $^{***}P<0.001$ vs. WT group, $^{\#}P<0.05$, $^{\#\#}P<0.01$ vs. APP/PS1 sh-NC group

target quadrant compared with age-matched APP/PS1 mice (Fig. 2G). There was no significant difference in swimming velocity (Fig. 2H). These findings suggest that UAF1 knockdown ameliorated cognitive deficits in APP/PS1 mice.

UAF1 Knockdown Decreased Aβ Burden and p-Tau Level in APP/PS1 Mice

In fig. 2, we found that knockdown of UAF1 improved cognitive impairment in AD mice by MWM experiment. Meanwhile, the accumulation of Aβ-derived from the amyloid precursor protein (APP) and tau proteins are the conventional pathologic features in the brain of the AD, which initiates a cascade of events involving PANoptosis (including pyroptosis, apoptosis, and necroptosis) and inflammation [15]. The deposition of Aβ plaques and tau tangles activates microglia, leading to neuroinflammation. Notably, sustained neuroinflammation exacerbate tau pathology, which in turn can aggravate inflammatory responses. The interplay between these processes creates a vicious cycle that accelerates neuronal damage and cognitive decline in AD [16]. Meanwhile, NF-κB/NLRP3 signal is the most clear and important signaling pathway that causes neuroinflammation [17]. Therefore, we examined the effect of knocking down UAF1 on the above indicators. As shown in Fig. 3A and B, UAF1 knockdown decreased Aβ burden and p-Tau levels in the cortex, CA1, and DG regions of APP/PS1 mice, as shown by immunofluorescence. We further examined APP, NLRP3, p-P65, Tau and p-Tau expression in the hippocampus of the two groups, the total tau protein had not changed, the other parameters were significantly downregulated in UAF1 knockdown group (Fig. 3C). Based on these observations, we inferred that UAF1 is involved in regulating Aβ and p-Tau. Overall, these results suggest that targeting UAF1 efficiently ameliorates pathology in APP/PS1 mice.

Knockdown of UAF1 Attenuated Neurotoxicity of SH-SY5Y Induced by $A\beta_{25-35}$

SH-SY5Y, a commonly used neuronal cell line, has been widely utilized to study neurodegenerative diseases with $A\beta_{25-35}$ treatment. Therefore, we selected SH-SY5Y cells as the in vitro model [18]. We first established a stable UAF1 knockdown SH-SY5Y cell line through lentiviral infection (Fig. 4A). Among the tested shRNAs, shRNA-2 demonstrated the strongest interference effect, leading to its selection for subsequent experiments. Previous studies have shown that Aβ affects neuronal viability [19, 20]. Compared to the control group, Aβ25−35 treatment partially suppressed cell OD, whereas UAF1 knockdown reversed cell viability inhibition to some extent (Fig. 4B). Similarly, colony formation assays confirmed that UAF1 knockdown increased the number of cell colonies (Fig. 4C). $A\beta_{25-35}$ has been shown to reduce cell viability through various forms of cell death, including apoptosis and pyroptosis [8, 21, 22]. To identify the specific mechanisms, we added the apoptosis inhibitor Z-VAD-FMK and the pyroptosis inhibitor VX-765. As shown in Fig.S3, inhibition of apoptosis and pyroptosis partially reversed $A\beta_{25-35}$ induced cytotoxicity in SH-SY5Y cells and UAF1 knockdown further rescued cell viability. We utilized flow cytometry to measure the apoptotic ratio across different groups. While the control group exhibited no obvious apoptosis, apoptotic cells increased following $A\beta_{25-35}$ treatment; however, UAF1 knockdown reduced the proportion of apoptotic cells in the $A\beta_{25-35}$-treated group (Fig. 4D). Additionally, a 2′,7′-dichlorofluorescin diacetate assay was performed to observe ROS levels. $A\beta_{25-35}$-treated cells exhibited high ROS production, but knockdown of UAF1 reduced ROS levels (Fig. 4E). These findings suggest that UAF1 knockdown protects against Aβ-induced neurotoxicity.

Knockdown of UAF1 Alleviated NLRP3 Mediated Pyroptosis in Vitro

The activation of the NF-κB and NLRP3 inflammasome pathways plays a crucial role in the AD pathological process by mediating pyroptosis [23, 24]. Aβ can activate the TLR4/NF-κB/NLRP3 signaling pathway and influence NLRP3 inflammasome-related proinflammatory cytokine levels in AD [17, 25]. p-P65, a marker of the active NF-κB/NLRP3 pathway, was first examined by immunofluorescence, which revealed stronger red fluorescence in the Aβ -treated group. However, UAF1 knockdown attenuated this fluorescence intensity (Fig. 5A). Next, we examined the effects of UAF1 on NLRP3-mediated inflammatory factors in SH-SY5Y cells. UAF1 knockdown notably decreased NLRP3 expression (Fig. 5B), and sh-UAF1 also reduced the generation of IL-1β and IL-18 (Fig. 5B and C). To quantitatively assess the impact of UAF1 on $A\beta_{25-35}$-induced pyroptosis, the levels of p-P65, NLRP3, GSDMD, and N-terminal GSDMD (GSDMD-N) in SH-SY5Y cells were analyzed. Consistent with previous data, the levels of p-P65 and NLRP3 were significantly reduced in the sh-UAF1 group (Fig. 5D). Pyroptosis is induced by active caspase-1, which cleaves the GSDMD full-length protein to release GSDME-N. As shown in Fig. 5D, $A\beta_{25-35}$ cleaved GSDME into GSDME-N in SH-SY5Y cells, and GSDME-N/GSDME was significantly up-regulated in the Aβ experimental group. However, sh-UAF1 reversed the cleavage action and alleviated pyroptosis (Fig. 5D). These findings suggest that UAF1 knockdown reduces $A\beta_{25-35}$-induced proinflammatory cytokine production and weakens NLRP3-mediated pyroptosis.

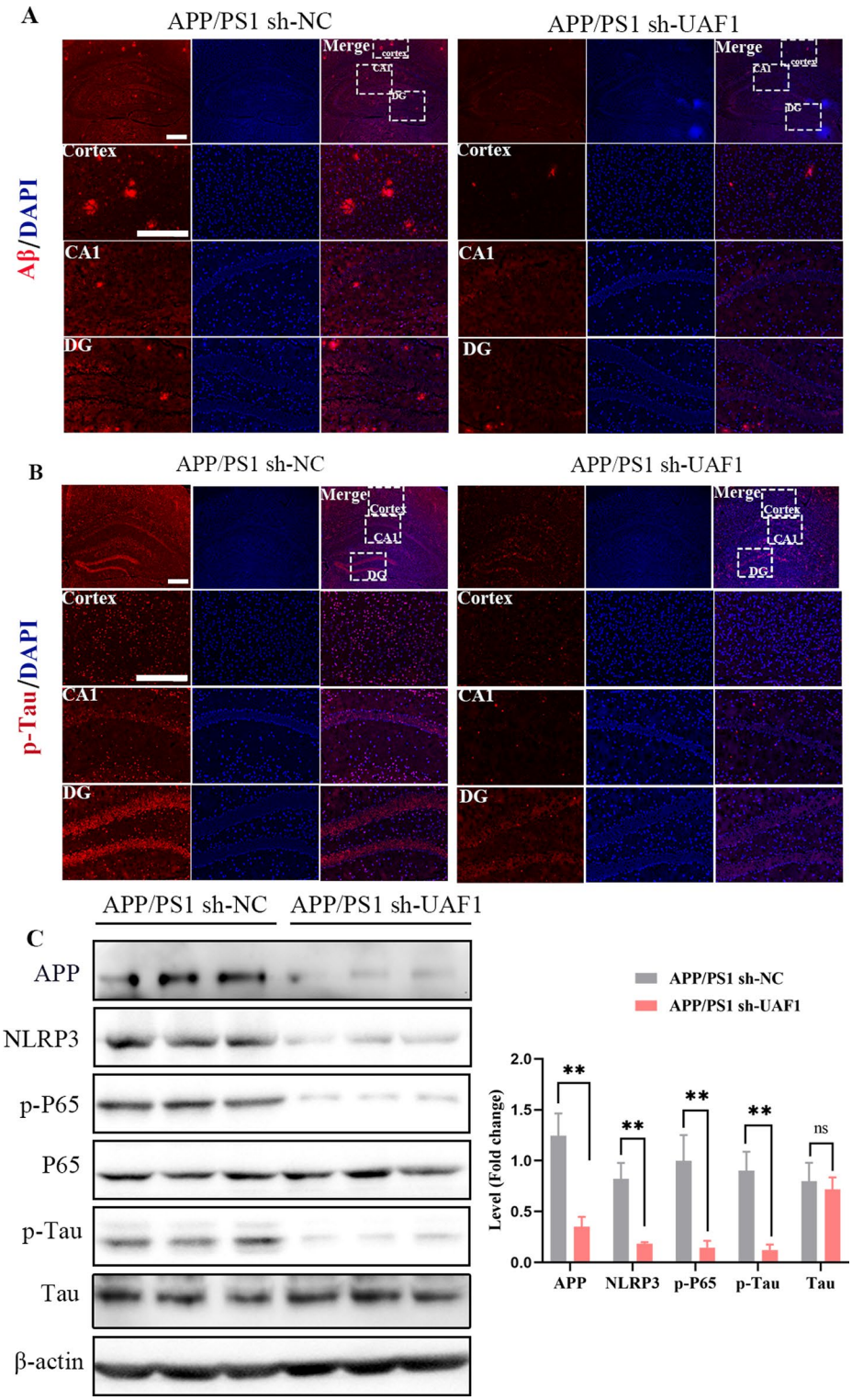

Fig. 3 UAF1 knockdown reduced Aβ deposit and p-Tau in APP/PS1 mice. AAV-sh-NC or AAV-sh-UAF1 was injected into the 5-month APP/PS1 mice by the brain stereotactic apparatus, four weeks later, obtained the brain tissue slices after MWM test. (**A**) Immunofluorescent images of Aβ (red) and DAPI (blue) in the cortex, CA1, and DG region from the sh-NC and sh-UAF1 mice. The white squares indicate that the corresponding regions are to be enlarged, the enlarged regions are the cortex, CA1 region and DG region in sequence. Scale bar, 100 μm (**B**) Immunofluorescent images of p-Tau (red) and DAPI (blue) in the cortex, CA1, and DG region from the sh-NC and sh-UAF1 mice. The white squares indicate that the corresponding regions are to be enlarged, the enlarged regions are the cortex, CA1 region and DG region in sequence. Scale bar, 100 μm (**C**) Immunoblots and quantification of APP, NLRP3, p-P65, P65, p-Tau and Tau expression in the in the hippocampus from APP/PS1 mice. ($n=6$ mice per group). Data are presented as mean ± S.D. Statistical significance: $^{**}p<0.01$ vs. sh-NC group

UAF1 Directly Interacted with NLRP3 and Suppresses its Ubiquitination-Mediated Degradation

To further explore how UAF1 influences NLRP3-mediated pyroptosis at the molecular level, we transfected SH-SY5Y cells with varying doses of UAF1. As shown in Fig. 6A, UAF1 upregulation significantly increased NLRP3 protein levels in a dose-dependent manner (Fig. 6A). Given the prediction of UAF1 binding to NLRP3, we co-transfected Flag-UAF1 and Myc-NLRP3 into SH-SY5Y cells. Through in vitro binding assays, we observed that UAF1

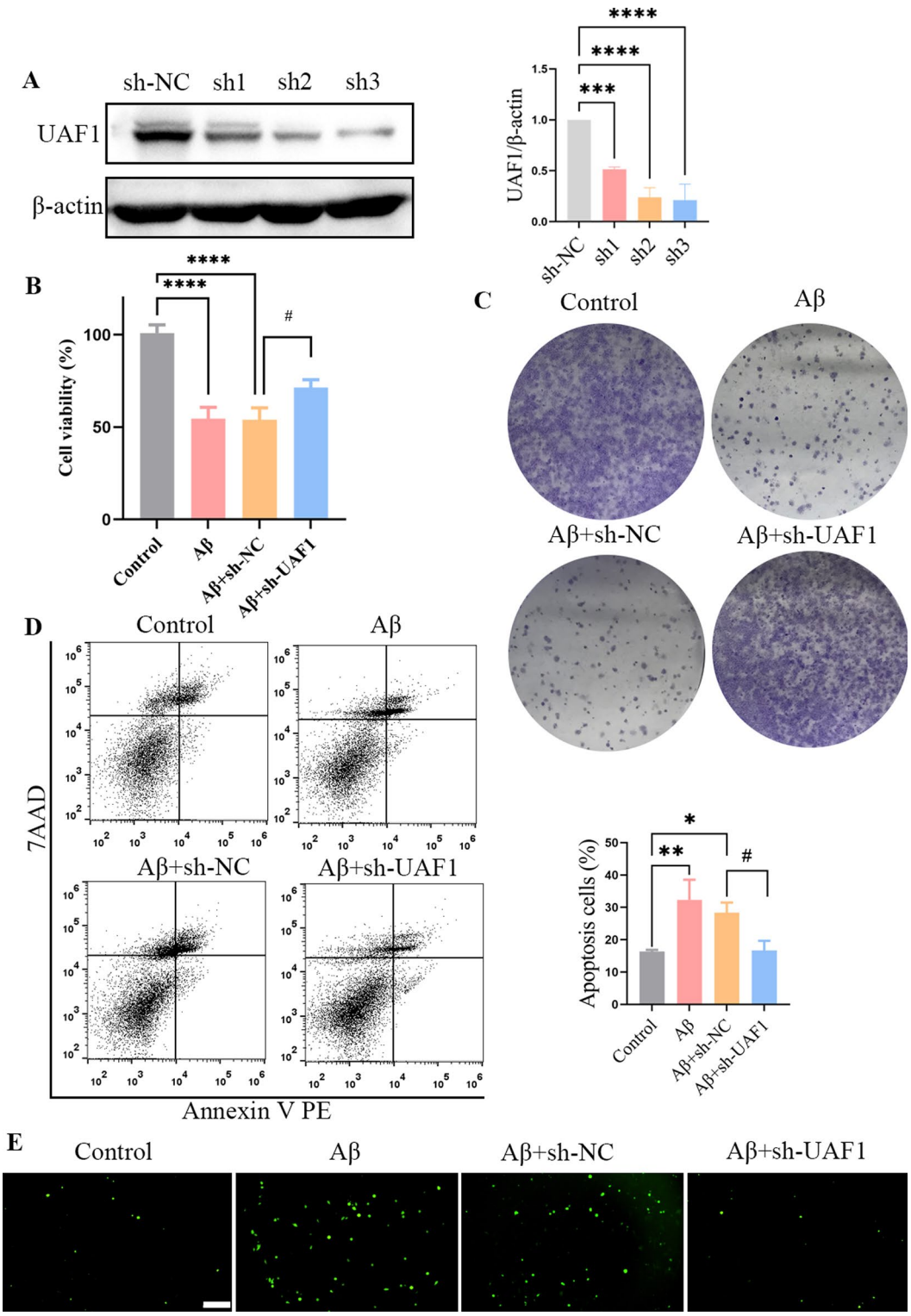

Fig. 4 The protective effect of UAF1 knockdown against Aβ-induced cytotoxicity. (**A**) Immunoblots and quantification of UAF1 knockdown efficiency. UAF1-silenced stable cell strain was obtained through infecting the lentivirus expressing inducible UAF1-shRNA and then selected with puromycin in SH-SY5Y cells. (**B**) Cell viability of SH-SY5Y cells in the control, sh-NC, and sh-UAF1 with or without $A\beta_{25\text{-}35}$ treatment group. (**C**) Colony formation test of SH-SY5Y cells in the different group. (**D**) FCM analyzed data for SH-SY5Y cells apoptosis in the different group. (**E**) The ROS levels of SH-SY5Ycells by the DCFH-DA fluorescent probe in the four group. Scale bar, 100 μm. The relevant experiments presented in this part were performed independently at least three times. Data are presented as mean ± S.D. Statistical significance: * $p<0.05$, ** $p<0.01$, *** $p<0.001$, **** $p<0.0001$ vs. Control group, $^{\#}P<0.05$ vs. Aβ + sh-NC group

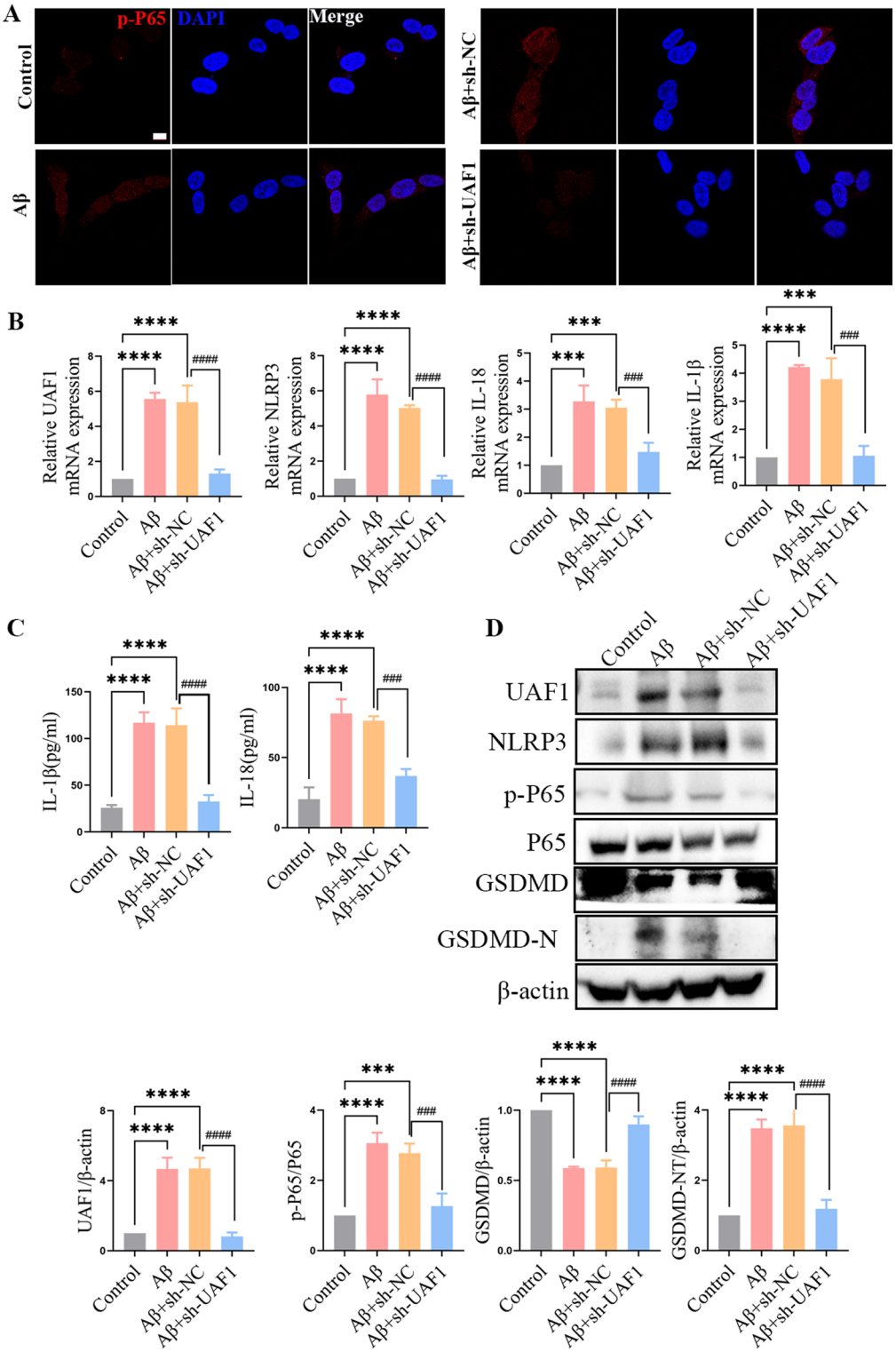

Fig. 5 UAF1 knockdown alleviated NLRP3 mediated pyroptosis. SH-SY5Y cells were transfected with lentivirus expressing inducible UAF1-shRNA, after puromycin screening, treated the stable cell strain with $A\beta_{25-35}$ for 24 h. (**A**) Immunofluorescent images of p-P65 (red) and DAPI (blue) in the four groups. Scale bar, 50 μm. (**B**) QRT-PCR analysis of UAF1, NLRP3, IL-1β, and IL-18 expression in the mRNA level. (**C**) ELISA analysis of IL-1β and IL-18 expression in the supernatant. (**D**) Immunoblots and quantification of UAF1, NLRP3, p-P65, P65, GSDMD, and GSDMD-N in the different groups. The relevant experiments presented in this part were performed independently at least three times. Data are presented as mean ± S.D. Statistical significance: $^{**}p<0.01$, $^{***}p<0.001$, $^{****}p<0.0001$ vs. Control group, $^{\#\#}P<0.01$, $^{\#\#\#}p<0.001$, $^{\#\#\#\#}p<0.0001$ vs. Aβ + sh-NC group

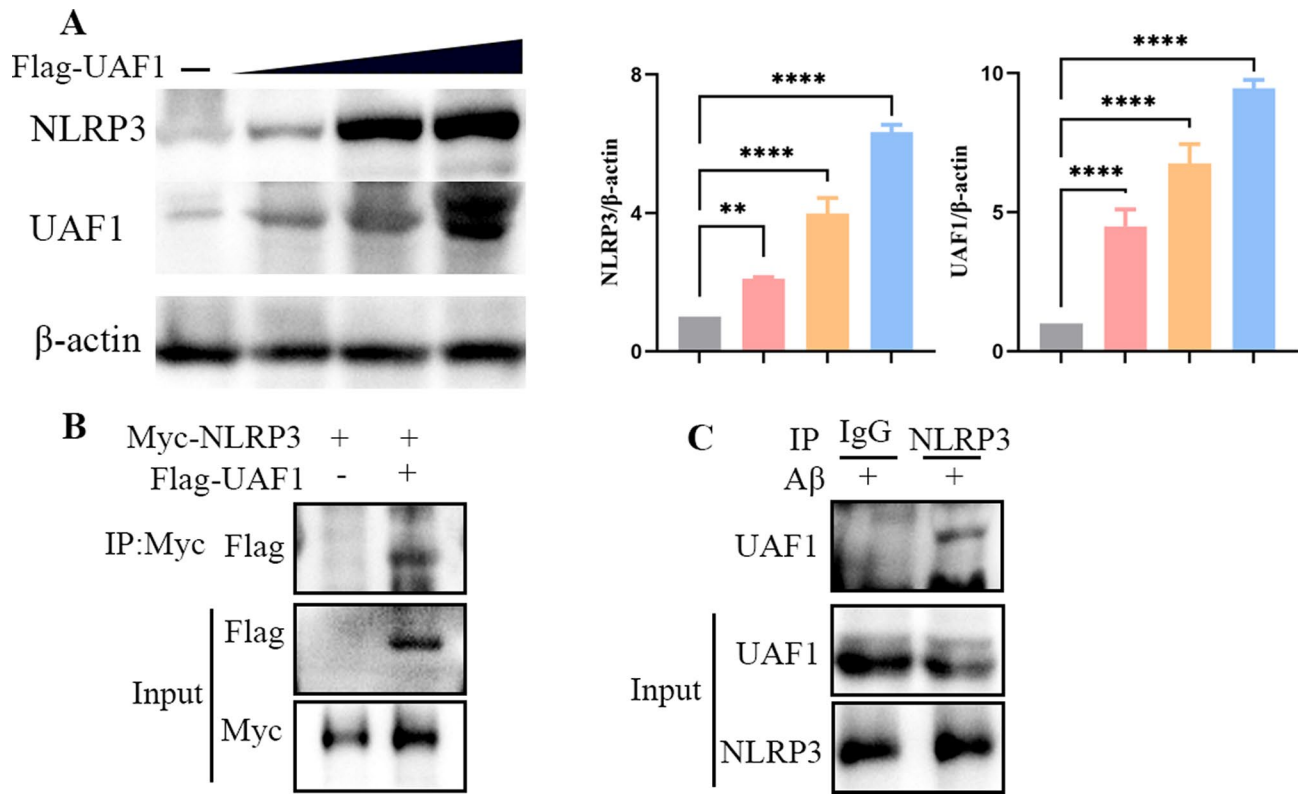

Fig. 6 UAF1 directly bound to NLRP3. (**A**) Immunoblots and quantification of NLRP3 and UAF1 expression. SH-SY5Y cells were transfected with an increasing amount of UAF1 expression plasmid. (**B**) Myc-NLRP3 and Flag-UAF1 were co-transfected into SH-SY5Y cells. Cell lysates were immunoprecipitated with an anti-Myc antibody and then immunoblotted with the indicated antibodies. (**C**) Co-immunoprecipitation of endogenous UAF1 with endogenous NLRP3 in SH-SY5Y cells stimulated with $A\beta_{25-35}$ for 24 h. The relevant experiments presented in this part were performed independently at least three times. Data are presented as mean ± S.D. Statistical significance: $^{**}p<0.01$, $^{***}p<0.001$, $^{****}p<0.0001$

coimmunoprecipitated with NLRP3 (Fig. 6B). Consistently, the endogenous interaction was also observed in SH-SY5Y cells subjected to $A\beta_{25-35}$ stimulation, where UAF1 interacted with NLRP3 following $A\beta_{25-35}$ treatment (Fig. 6C). Collectively, these results indicate that UAF1 specifically binds to NLRP3.

Discussion

In our study, we found that targeting UAF1 alleviate neurotoxicity by inhibiting APP/NLRP3 axis-mediated pyroptosis and apoptosis. Mechanistic analyses revealed that UAF1 directly binds to NLRP3. This binding influences the assembly and activation of the NLRP3 inflammasome, thereby affecting downstream inflammatory responses and pyroptosis. Meanwhile, in vivo experiments, we also found that UAF1 can down-regulate the expression of Aβ and p-Tau (Fig. 3), so the influence of UAF1 on NRLP3-mediated pyroptosis and apoptosis may also be related to this effection. As we known, Aβ and p-Tau has a multi-pathway effect, which can drive PANoptosis, a complex form that integrates multiple cell death pathways (including pyroptosis, apoptosis, and necroptosis) [15, 16]. In vivo, we also found that UAF1 can reverse apoptosis promoted by $Abeta_{25-35}$. But the molecular mechanism has not been elucidated in this study. Whether the regulation of apoptosis by UAF1 is also dependent on NLRP3 or Aβ expression needs further study. It has been shown that activation of the NLRP3 inflammasome can work synergistically with other inflammasome (e.g., AIM2, NLRC4) to form larger multiprotein complexes that drive PANoptosis [15, 16]. $Abeta_{25-35}$ can also cause cell apoptosis through various ways, such as mitochondrial damage [26]. In Fig. 4E, we truly found that knockdown of UAF1 reduced ROS production inducing by $A\beta_{25-35}$. However, whether UAF1 can reverse apoptosis by protecting mitochondria still needs further study.

Pyroptosis, a form of programmed cell death, has emerged as a key factor in neurodegenerative diseases, including AD [5, 27]. The NLRP3 inflammasome serves as a pivotal canonical regulator of pyroptotic cell death in response to various stimuli, including Aβ aggregates, which are hallmark pathological features of AD [28–30]. In the context of AD, both Aβ and Tau oligomers can trigger

NLRP3 activation, leading to pyroptosis [31, 32]. Undoubtedly, NLRP3-mediated pyroptosis has become an important target for AD research and treatment. Recent studies have proposed that CRID3 binds to the NACHT domain of NLRP3 to inhibit its activity [33]. This binding effectively inhibited both Aβ-induced and Tau-induced activation of the NLRP3 inflammasome [32–35], thereby decreasing IL-1β release and Tau seeding, ultimately ameliorating memory impairments [33, 34]. Additionally, P62, an autophagy-related protein, recognizes and binds to ubiquitin-modified NLRP3, reducing the pro-inflammatory state, mitigating microglial pyroptosis, and ultimately improving cognitive function in AD [2]. Recently, a growing number of studies have focused on glial cell-mediated pyroptosis, whereas research on the connection between neurons and pyroptosis remains limited. A recent study reported that the NLRP3 and NLRP1 inflammasomes can induce neuroinflammatory processes via pyroptosis in neurons [36]. $A\beta_{1-42}$ triggers pyroptosis through the GSDMD protein in neurons, and the NLRP3/caspase-1 pathway regulates GSDMD cleavage [7]. It has also been reported that Aβ upregulates NLRP3, ASC, and caspase-1 expression, resulting in the production of proinflammatory factors and neuronal pyroptosis in SH-SY5Y cells [37–39]. Targeting the inhibition of pyroptosis significantly attenuated Aβ-induced neurotoxic effects and malignant neuroblastoma [7, 38]. Furthermore, a published report demonstrated that p-Tau induces pyroptosis in PC12 cells [39]. Consistently, we have demonstrated that $A\beta_{25-35}$ upregulates UAF1 expression. In vitro experiments using neuronal cell lines exposed to Aβ revealed that UAF1 knockdown reduced the activation of the NLRP3 inflammasome. This reduction in NLRP3 activity correlated with decreased production of inflammatory factors. Consequently, the extent of pyroptosis was diminished, resulting in increased cell viability and reduced neurotoxicity. These findings underscore the protective role of UAF1 knockdown against Aβ-triggered inflammatory responses and cellular damage in neurons.

Evidence suggests that the APP/PS1 transgenic mouse model, which overproduces mutant forms of APP and PS1, is widely used to study AD. These mice exhibit Aβ plaque deposition, hyperphosphorylated Tau aggregates, neuroinflammation, and cognitive deficits similar to those observed in patients with AD [40, 41]. In our study, we also observed the phenotypic changes described above, which are also consistent with previous reports [42, 43]. The expression changes on Tau and phospho-tau are complex in APP/PS1 transgenic mouse model and AD patients. Recent cross-sectional and longitudinal imaging studies report that neocortical Aβ amyloidosis precedes the accumulation of Tau aggregates. This means fibrillar Aβ upstream of neocortical tau, and points towards the existence of complex and dynamic links between the two pathognomonic features of AD [44, 45]. Meanwhile, plaque-associated neuritic tau has been reported to be closely related its post-translational modifications, particularly its phosphorylated state [46]. In our study, we demonstrated that UAF1 knockdown in APP/PS1 mice significantly reduces Aβ plaque burden, phospho-tau and downstream neuroinflammation. Mechanistic analyses revealed that UAF1 directly binds to NLRP3 and activation of the NLRP3 inflammasome, but the affection of UAF1 on Aβ and phospho-tau expression has not been elucidated and need further study.

In summary, the above results highlight UAF1 as a potential therapeutic target for AD. Future research should focus on elucidating the precise molecular mechanisms of the UAF1-NLRP3 interaction and developing strategies to modulate this pathway in vivo. The interaction between UAF1 and NLRP3 and its influence on pyroptosis provide valuable insights into the mechanisms underlying AD progression. Such advancements could pave the way for novel therapeutic approaches aimed at mitigating neuroinflammation and cell death in AD, ultimately improving patient outcomes.

Supplementary Information The online version contains supplementary material available at https://doi.org/10.1007/s11064-025-04379-x.

Acknowledgements The coauthors thank the laboratory research team members at the Second Hospital of Shandong University for their professional assistance.

Author Contributions L C, F L and Z X: conceived and designed research, formal analysis, wrote the manuscript, edited the text, Conceptualization. X M, D T, B Z, Y X, X Z, Y X, H Y, J B: helped with experiments, collection and assembly of data. L C, F L and Z X: Writing & Editing. All authors reviewed the manuscript.

Funding This study was financially supported by the National Natural Science Foundation of China (81870848), the Shandong University Multidisciplinary Research and Innovation Team of Young Scholars(2020QNQT019), the Fundamental Research Funds of the Chinese Academy of Medical Sciences(2019-RC-HL-026), and the Natural Science Foundation of Shandong Province (ZR2023MH340).

Data Availability No datasets were generated or analysed during the current study.

Code Availability Not applicable.

Declarations

Ethical Approval The Animal Ethics Committee of the Second Hospital of Shandong University approved this study in accordance with the National Institutes of Health guidelines for the Care and Use of Laboratory Animals (Ethics approval No. KYLL-2021(KJ)A-0195).

Consent to Participate Not applicable.

Consent for Publication Not applicable.

Competing Interests The authors declare no competing interests.

References

1. Hu B, Zhang J, Huang J, Luo B, Zeng X, Jia J (2024) NLRP3/1-mediated pyroptosis: beneficial clues for the development of novel therapies for Alzheimer's disease. Neural Regen Res 19:2400–2410. https://doi.org/10.4103/1673-5374.391311
2. Moonen S, Koper MJ, Van Schoor E, Schaeverbeke JM, Vandenberghe R, von Arnim CAF, Tousseyn T, De Strooper B, Thal DR (2023) Pyroptosis in Alzheimer's disease: cell type-specific activation in microglia, astrocytes and neurons. Acta Neuropathol 145:175–195. https://doi.org/10.1007/s00401-022-02528-y
3. Friker LL, Scheiblich H, Hochheiser IV, Brinkschulte R, Riedel D, Latz E, Geyer M, Heneka MT (2020) beta-Amyloid clustering around ASC fibrils boosts its toxicity in microglia. Cell Rep 30:3743–3754e3746. https://doi.org/10.1016/j.celrep.2020.02.025
4. Huang C, Dong D, Jiao Q, Pan H, Ma L, Wang R (2017) Sarsasapogenin-AA13 ameliorates Abeta-induced cognitive deficits via improving neuroglial capacity on Abeta clearance and antiinflammation. CNS Neurosci Ther 23:498–509. https://doi.org/10.1111/cns.12697
5. Cai Y, Chai Y, Fu Y, Wang Y, Zhang Y, Zhang X, Zhu L, Miao M, Yan T (2021) Salidroside ameliorates Alzheimer's disease by targeting NLRP3 Inflammasome-Mediated pyroptosis. Front Aging Neurosci 13:809433. https://doi.org/10.3389/fnagi.2021.809433
6. Vontell RT, de Rivero Vaccari JP, Sun X, Gultekin SH, Bramlett HM, Dietrich WD, Keane RW (2023) Identification of inflammasome signaling proteins in neurons and microglia in early and intermediate stages of Alzheimer's disease. Brain Pathol 33:e13142. https://doi.org/10.1111/bpa.13142
7. Nopparat C, Boontor A, Kutpruek S, Govitrapong P (2023) The role of melatonin in amyloid beta-induced inflammation mediated by inflammasome signaling in neuronal cell lines. Sci Rep 13:17841. https://doi.org/10.1038/s41598-023-45220-1
8. Meng X, Song Q, Liu Z, Liu X, Wang Y, Liu J (2024) Neurotoxic beta-amyloid oligomers cause mitochondrial dysfunction-the trigger for PANoptosis in neurons. Front Aging Neurosci 16:1400544. https://doi.org/10.3389/fnagi.2024.1400544
9. Li J, Zhuang L, Luo X, Liang J, Sun E, He Y (2020) Protection of MCC950 against Alzheimer's disease via inhibiting neuronal pyroptosis in SAMP8 mice. Exp Brain Res 238:2603–2614. https://doi.org/10.1007/s00221-020-05916-6
10. Yu Z, Song H, Jia M, Zhang J, Wang W, Li Q, Zhang L, Zhao W (2017) USP1-UAF1 deubiquitinase complex stabilizes TBK1 and enhances antiviral responses. J Exp Med 214:3553–3563. https://doi.org/10.1084/jem.20170180
11. Song H, Zhao C, Yu Z, Li Q, Yan R, Qin Y, Jia M, Zhao W (2020) UAF1 deubiquitinase complexes facilitate NLRP3 inflammasome activation by promoting NLRP3 expression. Nat Commun 11:6042. https://doi.org/10.1038/s41467-020-19939-8
12. Zhu Y, Zhang M, Wang J, Wang Q (2022) Knockdown of UAF1 alleviates sevoflurane-induced cognitive impairment and neurotoxicity in rats by inhibiting pro-inflammatory signaling and oxidative stress. J Toxicol Sci 47:349–357. https://doi.org/10.2131/jts.47.349
13. Liu Y, Qin K, Dou K, Ren J, Hou B, Xie A (2025) TMEM106B knockdown exhibits a neuroprotective effect in Parkinson's disease models via regulating autophagy-lysosome pathway. Biochim Biophys Acta Mol Basis Dis 1871:167553. https://doi.org/10.1016/j.bbadis.2024.167553
14. Wang L, Zhao M (2022) Suppression of NOD-like receptor protein 3 inflammasome activation and macrophage M1 polarization by Hederagenin contributes to Attenuation of sepsis-induced acute lung injury in rats. Bioengineered 13:7262–7276. https://doi.org/10.1080/21655979.2022.2047406
15. Chen Y, Yu Y (2023) Tau and neuroinflammation in Alzheimer's disease: interplay mechanisms and clinical translation. J Neuroinflammation 20:165. https://doi.org/10.1186/s12974-023-02853-3
16. Zhuang X, Lin J, Song Y, Ban R, Zhao X, Xia Z, Wang Z, Zhang G (2024) The interplay between accumulation of Amyloid-Beta and Tau proteins, PANoptosis, and inflammation in Alzheimer's disease. Neuromolecular Med 27:2. https://doi.org/10.1007/s12017-024-08815-z
17. McManus RM, Latz E (2024) NLRP3 inflammasome signalling in Alzheimer's disease. Neuropharmacology 252:109941. https://doi.org/10.1016/j.neuropharm.2024.109941
18. Yu X, Tao J, Xiao T, Duan X (2024) P-hydroxybenzaldehyde protects caenorhabditis elegans from oxidative stress and beta-amyloid toxicity. Front Aging Neurosci 16:1414956. https://doi.org/10.3389/fnagi.2024.1414956
19. Guo S, Lei Q, Guo H, Yang Q, Xue Y, Chen R (2023) Edaravone attenuates Abeta 1-42-Induced inflammatory damage and ferroptosis in HT22 cells. Neurochem Res 48:570–578. https://doi.org/10.1007/s11064-022-03782-y
20. Kam TI, Song S, Gwon Y, Park H, Yan JJ, Im I, Choi JW, Choi TY, Kim J, Song DK, Takai T, Kim YC, Kim KS, Choi SY, Choi S, Klein WL, Yuan J, Jung YK (2013) FcgammaRIIb mediates amyloid-beta neurotoxicity and memory impairment in Alzheimer's disease. J Clin Invest 123:2791–2802. https://doi.org/10.1172/JCI66827
21. Shen YX, Xu SY, Wei W, Wang XL, Wang H, Sun X (2002) Melatonin blocks rat hippocampal neuronal apoptosis induced by amyloid beta-peptide 25–35. J Pineal Res 32:163–167. https://doi.org/10.1034/j.1600-079x.2002.1o839.x
22. Jia J, Liu H, Sun L, Xu Y, Zeng X (2024) Correction: Thioredoxin-1 protects neurons through inhibiting NLRP1-Mediated neuronal pyroptosis in models of Alzheimer's disease. Mol Neurobiol. https://doi.org/10.1007/s12035-024-04523-8
23. Saresella M, La Rosa F, Piancone F, Zoppis M, Marventano I, Calabrese E, Rainone V, Nemni R, Mancuso R, Clerici M (2016) The NLRP3 and NLRP1 inflammasomes are activated in Alzheimer's disease. Mol Neurodegener 11:23. https://doi.org/10.1186/s13024-016-0088-1
24. Yang J, Wise L, Fukuchi KI (2020) TLR4 Cross-Talk with NLRP3 inflammasome and complement signaling pathways in Alzheimer's disease. Front Immunol 11:724. https://doi.org/10.3389/fimmu.2020.00724

25. Rui W, Xiao H, Fan Y, Ma Z, Xiao M, Li S, Shi J (2021) Systemic inflammasome activation and pyroptosis associate with the progression of amnestic mild cognitive impairment and Alzheimer's disease. J Neuroinflammation 18:280. https://doi.org/10.1186/s12974-021-02329-2
26. McGill Percy KC, Liu Z, Qi X (2025) Mitochondrial dysfunction in Alzheimer's disease: Guiding the path to targeted therapies. https://doi.org/10.1016/j.neurot.2025.e00525. Neurotherapeutics:e00525
27. Han C, Hu Q, Yu A, Jiao Q, Yang Y (2021) Mafenide derivatives inhibit neuroinflammation in Alzheimer's disease by regulating pyroptosis. J Cell Mol Med 25:10534–10542. https://doi.org/10.1111/jcmm.16984
28. Van Zeller M, Dias D, Sebastiao AM, Valente CA (2021) NLRP3 inflammasome: A starring role in Amyloid-beta- and Tau-Driven pathological events in Alzheimer's disease. J Alzheimers Dis 83:939–961. https://doi.org/10.3233/JAD-210268
29. Ising C, Venegas C, Zhang S, Scheiblich H, Schmidt SV, Vieira-Saecker A, Schwartz S, Albasset S, McManus RM, Tejera D, Griep A, Santarelli F, Brosseron F, Opitz S, Stunden J, Merten M, Kayed R, Golenbock DT, Blum D, Latz E, Buee L, Heneka MT (2019) NLRP3 inflammasome activation drives Tau pathology. Nature 575:669–673. https://doi.org/10.1038/s41586-019-1769-z
30. Halle A, Hornung V, Petzold GC, Stewart CR, Monks BG, Reinheckel T, Fitzgerald KA, Latz E, Moore KJ, Golenbock DT (2008) The NALP3 inflammasome is involved in the innate immune response to amyloid-beta. Nat Immunol 9:857–865. https://doi.org/10.1038/ni.1636
31. Coll RC, Hill JR, Day CJ, Zamoshnikova A, Boucher D, Massey NL, Chitty JL, Fraser JA, Jennings MP, Robertson AAB, Schroder K (2019) MCC950 directly targets the NLRP3 ATP-hydrolysis motif for inflammasome Inhibition. Nat Chem Biol 15:556–559. https://doi.org/10.1038/s41589-019-0277-7
32. Luciunaite A, McManus RM, Jankunec M, Racz I, Dansokho C, Dalgediene I, Schwartz S, Brosseron F, Heneka MT (2020) Soluble Abeta oligomers and protofibrils induce NLRP3 inflammasome activation in microglia. J Neurochem 155:650–661. https://doi.org/10.1111/jnc.14945
33. Dempsey C, Rubio Araiz A, Bryson KJ, Finucane O, Larkin C, Mills EL, Robertson AAB, Cooper MA, O'Neill LAJ, Lynch MA (2017) Inhibiting the NLRP3 inflammasome with MCC950 promotes non-phlogistic clearance of amyloid-beta and cognitive function in APP/PS1 mice. Brain Behav Immun 61:306–316. https://doi.org/10.1016/j.bbi.2016.12.014
34. Stancu IC, Cremers N, Vanrusselt H, Couturier J, Vanoosthuyse A, Kessels S, Lodder C, Brone B, Huaux F, Octave JN, Terwel D, Dewachter I (2019) Aggregated Tau activates NLRP3-ASC inflammasome exacerbating exogenously seeded and non-exogenously seeded Tau pathology in vivo. Acta Neuropathol 137:599–617. https://doi.org/10.1007/s00401-018-01957-y
35. Zhang D, Zhang Y, Pan J, Cao J, Sun X, Li X, Zhang L, Qin C (2023) Degradation of NLRP3 by p62-dependent-autophagy improves cognitive function in Alzheimer's disease by maintaining the phagocytic function of microglia. CNS Neurosci Ther 29:2826–2842. https://doi.org/10.1111/cns.14219
36. Bai Y, Liu D, Zhang H, Wang Y, Wang D, Cai H, Wen H, Yuan G, An H, Wang Y, Shi T, Wang Z (2021) N-salicyloyl tryptamine derivatives as potential therapeutic agents for Alzheimer's disease with neuroprotective effects. Bioorg Chem 115:105255. https://doi.org/10.1016/j.bioorg.2021.105255
37. Wang Q, Guo S, Hu D, Dong X, Meng Z, Jiang Y, Feng Z, Zhou W, Song W (2024) Enhanced Gasdermin-E-mediated pyroptosis in Alzheimer's disease. Neuroscience 536:1–11. https://doi.org/10.1016/j.neuroscience.2023.11.004
38. Zhao N, Sun C, Zheng M, Liu S, Shi R (2019) Amentoflavone suppresses amyloid beta1-42 neurotoxicity in Alzheimer's disease through the Inhibition of pyroptosis. Life Sci 239:117043. https://doi.org/10.1016/j.lfs.2019.117043
39. Li Y, Xu P, Shan J, Sun W, Ji X, Chi T, Liu P, Zou L (2020) Interaction between hyperphosphorylated Tau and pyroptosis in forskolin and streptozotocin induced AD models. Biomed Pharmacother 121:109618. https://doi.org/10.1016/j.biopha.2019.109618
40. Dhapola R, Kumari S, Sharma P, HariKrishnaReddy D (2023) Insight into the emerging and common experimental in-vivo models of Alzheimer's disease. Lab Anim Res 39:33. https://doi.org/10.1186/s42826-023-00184-1
41. Sasaguri H, Nilsson P, Hashimoto S, Nagata K, Saito T, De Strooper B, Hardy J, Vassar R, Winblad B, Saido TC (2017) APP mouse models for Alzheimer's disease preclinical studies. EMBO J 36:2473–2487. https://doi.org/10.15252/embj.201797397
42. Natunen T, Martiskainen H, Marttinen M, Gabbouj S, Koivisto H, Kemppainen S, Kaipainen S, Takalo M, Svobodova H, Leppanen L, Kemilainen B, Ryhanen S, Kuulasmaa T, Rahunen E, Juutinen S, Makinen P, Miettinen P, Rauramaa T, Pihlajamaki J, Haapasalo A, Leinonen V, Tanila H, Hiltunen M (2020) Diabetic phenotype in mouse and humans reduces the number of microglia around beta-amyloid plaques. Mol Neurodegener 15:66. https://doi.org/10.1186/s13024-020-00415-2
43. Abad S, Ramon-Duaso C, Lopez-Arnau R, Folch J, Pubill D, Camarasa J, Camins A, Escubedo E (2019) Effects of MDMA on neuroplasticity, amyloid burden and phospho-tau expression in APPswe/PS1dE9 mice. J Psychopharmacol 33:1170–1182. https://doi.org/10.1177/0269881119855987
44. Lee WJ, Brown JA, Kim HR, La Joie R, Cho H, Lyoo CH, Rabinovici GD, Seong JK, Seeley WW, Alzheimer's Disease Neuroimaging I (2022) Regional Abeta-tau interactions promote onset and acceleration of Alzheimer's disease Tau spreading. Neuron 110:1932–1943. https://doi.org/10.1016/j.neuron.2022.03.034. e1935
45. Jacobs HIL, Hedden T, Schultz AP, Sepulcre J, Perea RD, Amariglio RE, Papp KV, Rentz DM, Sperling RA, Johnson KA (2018) Structural tract alterations predict downstream Tau accumulation in amyloid-positive older individuals. Nat Neurosci 21:424–431. https://doi.org/10.1038/s41593-018-0070-z
46. Stefanoska K, Gajwani M, Tan ARP, Ahel HI, Asih PR, Volkerling A, Poljak A, Ittner A (2022) Alzheimer's disease: ablating single master site abolishes Tau hyperphosphorylation. Sci Adv 8:eabl8809. https://doi.org/10.1126/sciadv.abl8809